PCCP

A study of $FeCO^+$ with correlated wavefunctions

Kurt R. Glaesemann,[a] Mark S. Gordon*[a] and Haruyuki Nakano[b]

[a] *Chemistry Department, Iowa State University, Ames Laboratory—United States Department of Energy, Ames, Iowa 50011, United States of America*
[b] *Department of Applied Chemistry, Graduate School of Engineering, University of Tokyo, 7-3-1 Hongo, Bunkyo-ku, Tokyo 113-8656, Japan*

Received 3rd November 1998, Accepted 4th January 1999

A study of $FeCO^+$ and Fe^+ using both the second-order multi-configurational quasi-degenerate perturbation theory (MC-QDPT2) method and the coupled cluster theory with single and double replacements (augmented by perturbative triples) [CCSD(T)] method are presented. An all-electron triple-ζ valence plus polarization basis set was used in all calculations. The equilibrium CCSD(T) geometry of $FeCO^+$ is found to be linear ($^4\Sigma^-$) with a Fe^+ to CO distance of 1.905 Å and a CO bond distance of 1.133 Å. The dissociation energy D_0 of $^4\Sigma^-$ $FeCO^+$ to ^{6}D Fe^+ and $^1\Sigma^+$ CO is predicted to be 28.8 kcal mol^{-1}, which is within the experimental range. Excited state properties including potential energy surfaces and D_e are predicted for the low lying sextet and quartet states of $FeCO^+$. The first excited state is predicted to be $^4\Delta$ with a D_e of 17.6 kcal mol^{-1}. The lowest sextet state is predicted to be $^6\Delta$ with a D_0 of 12.3 kcal mol^{-1}. Several examples of pathological behavior at many levels of theory have been discovered and are discussed.

I Introduction and background

CO is important in the chemistry of transition metals such as Fe^+, playing a role in many chemical processes and industrial procedures.[1–3] Hurlburt *et al.*[3] pointed out that there are thousands of literature citations that include the phrase "metal carbonyl".[4] In the oxidative addition of H_2 to metals and the reductive elimination of H_2 from metals,[5] CO is important because it effectively stabilizes transition metals, even those that carry negative charges.[1] The detailed nature of the CO wavefunction has been studied experimentally using electron momentum spectroscopy.[6] Besides Fe^+, CO has been experimentally studied interacting with Ag^+,[3,7] Cu^+,[7] V^+,[8] W^+,[9,10] Fe^-,[11,12] Fe,[12] Ni^-,[11] Cr^+,[10] Mo^+,[10] and Co^+,[13] using diffraction,[3] spectroscopy,[3] collision-induced dissociation (CID) in a guided ion beam tandem mass spectrometer,[7,8,13,14] energy resolved CID,[11] negative ion photoelectron spectroscopy,[12] molecular beam photoionization mass spectroscopy,[10] and Fourier transform ion cyclotron resonance mass spectrometry.[9]

$FeCO^+$ has been studied as a catalyst for reactions involving polyhalogenated methane and halogens both in a microwave discharge and without microwaves.[15] This capability makes $FeCO^+$ of particular interest given the role that halogens play in the atmospheric destruction of the ozone layer.[16] Gas phase studies and theoretical calculations have shown that $FeCO^+$ has significantly different reactivity and selectivity than Fe^+ and other complexes such as $Fe(H_2O)_n^+$.[17–19] Tjelta and Armentrout found that $FeCO^+$ activates both C—C and C—H bonds in ethane, while $Fe(H_2O)^+$ preferentially activates the C—H bonds.[20] This selectivity can be partially explained by the observation that R groups must interact with the 3d σ orbital in $Fe(H_2O)^+$ instead of the empty 4s orbital in $Fe(CO)^+$.[20] The photodissociation of $Fe(CO)_5$ has been studied with femtosecond lasers. $FeCO^+$ plays an important role in this reaction as the final intermediate, and as the reactant in the slowest step of the mechanism.[21] Careful study of the velocity distribution in the $Fe(CO)_5$ dissociation has also proved useful in analyzing the mechanism.[22] Majima found that using a transversely excited atmospheric (TEA) CO_2 laser to dissociate $Fe(CO)_5$ in the presence of SF_6 resulted in no $FeCO^+$ ion formation, and the loss of the first CO was the rate determining step.[23]

The ground state of $FeCO^+$ is consistently reported to be a quartet with $C_{\infty v}$ symmetry,[24–26] although that of Fe^+ is experimentally known to be a sextet[27] and that of CO is a singlet. None of the experimental or theoretical studies predict $COFe^+$ as the ground state geometry, although neutralization–reionization mass spectrometry (NRMS) had small FeO^+ fragment peaks implying that some $COFe^+$ was present.[28]

A wide variety of experimental studies have been carried out on $FeCO^+$. Selected ion flow tubes (SIFT) and collision-induced dissociation (CID) have proven effective in measuring bond dissociation energies (D_0) of Fe^+ containing compounds such as $Fe(N_2)_n^+$,[29] $Fe(CH_2O)_n^+$,[30] and $FeCO^+$.[29,31,32] CID gives a $FeCO^+$ D_0 of 36.1 $\pm$ 1.8 kcal mol^{-1} relative to ^{4}F Fe^+ and ground state CO. Vibrationally corrected CID gives a D_0 of 30.9 $\pm$ 0.9 kcal mol^{-1},[29] relative to ^{6}D Fe^+. Product kinetic energy release distributions (KERDS) gives a D_0 of 31.8 $\pm$ 3 kcal mol^{-1},[33] relative to ^{6}D Fe^+. Fourier transform mass spectrometry results were analyzed with Cook's kinetic method to give D_0 relative to $Fe(C_2H_4)^+$, yielding $D_0(FeCO^+)$ = 31.2 $\pm$ 0.2 kcal mol^{-1},[19] relative to an unspecified state of Fe^+. Ng *et al.* have studied $FeCO^+$ using photoelectron–photoion coincidence (PEPICO) and determined the D_0 of $Fe(CO)_n^+$ to be 17.8 $\pm$ 0.9, 25.2 $\pm$ 1.1, 25.7 $\pm$ 1.4, 41.5 $\pm$ 1.6, and 39.3 $\pm$ 2.0 kcal mol^{-1} for n = 5, 4, 3, 2, 1 respectively,[14] relative to ^{6}D Fe^+. PEPICO introduces $Fe(CO)_5$ into the photoionization region using a supersonic expansion to reduce rotational and vibrational scattering.[34–37] In the work of Ng *et al.*, relative PEPICO intensities for $Fe(CO)_n^+$ had to be estimated for n = 2, 1, 0. The primary focus of that work was on getting good relative intensities. In addition to PEPICO, Ng *et al.* used CID to study $FeCO^+$. $FeCO^+$ ions were selected with quadrupole mass

spectroscopy (QMS) and then collided with Ar to induce dissociation. The ratio of $FeCO^+$ reactant ions and Fe^+ product ions was analyzed with QMS, to give a D_0 of 33 ± 4 kcal mol^{-1} for $FeCO^+$,[14] relative to ^6D Fe^+. Since the PEPICO value is just an estimate, the experimental range for D_0 to ground state ^6D Fe^+ and CO is 30.9–33.0 kcal mol^{-1} with experimental error bars out to 28.8–37.0 kcal mol^{-1}. D_0 for dissociation to ^4F Fe^+ should be 5.35 kcal mol^{-1} larger than this range; that is, the experimental range for dissociation to ^4F Fe^+ is 34.15–42.35 kcal mol^{-1}.

The ground state of $FeCO^+$ has been investigated using many different theoretical methods, giving a wide range of dissociation energies. It is important to note that experiments measure D_0, while many calculations predict D_e values. D_e values are always slightly larger than D_0 values; in Section III, this difference is predicted to be 0.95 kcal mol^{-1} for $^4\Sigma^-$ $FeCO^+$.

The density functional theory (DFT) hybrid functional B3LYP[38] predicts a $FeCO^+$ binding energy of $D_e = 37.0$ kcal mol^{-1} relative to ^4F Fe^+ that is within the experimental error bars, unlike BLYP ($D_e = 47.8$ kcal mol^{-1}) and LSDA ($D_e =$ 50 kcal mol^{-1}).[24] The modified coupled pair functional (MCPF) predicts a binding energy (28.9 kcal mol^{-1}) that is too small.[24] Single-reference MP2 predicts 30.8 kcal mol^{-1} [25] which is also too low. Others have calculated the D_e for dissociation relative to ^6D Fe^+. This D_e is predicted by B3LYP to be 32.7 kcal mol^{-1},[39] which is within the experimental range. The previous calculations predict little significant charge transfer from Fe^+ to CO, and they demonstrate that an explicit treatment of correlation is essential to get proper energetics and geometries for $FeCO^+$,[40] as well as for $FeCO^-$[41] and FeCO.[26,42,43]

Studying multiple electronic states often requires a multi-configurational wavefunction. The investigation of multiple potential energy surfaces (PES) frequently requires the use of state-averaged (SA) wavefunctions to obtain a consistent treatment of the various electronic, and especially degenerate, states. A proper description of such species often requires more than a single, simple Lewis structure.[44] This requirement reduces the utility of DFT methods, except for those that implement one of the fractional occupation number (FON) formalisms[45–48] or the DFT CI singles formalism.[49] In this work the low lying quartet and sextet states of $FeCO^+$ are studied using multi-configurational self-consistent field (MCSCF)[50] wavefunctions, second-order multi-configurational quasi-degenerate perturbation theory (MC-QDPT2),[51–53] and single-configuration coupled cluster theory with single and double replacements, augmented by perturbative triples [CCSD(T)].[54] In Section II the theoretical approaches used to study Fe^+ and $FeCO^+$ are explained in detail. In Section III Fe^+ is examined with several different methods and basis sets. In Section IV $FeCO^+$ PES are studied and frequencies of the lowest sextet and quartet equilibrium geometries are presented. In Section V the possible origins of poor behavior in multi-reference perturbation theory are discussed in detail.

II Theoretical methods

$FeCO^+$, CO, and Fe^+ were studied using an all-electron triple-ζ valence plus polarization (TZVP) basis set. For Fe, a [10s6p] contraction of Wachters' (14s9p) primitive basis[55] was supplemented with the [3d] contraction of (6d) primitives proposed by Rappé *et al.*[56] This basis set was augmented with two sets of p functions ($\zeta = 0.231$ and $\zeta = 0.0899$) to give an adequate representation of the 4p subshell. This is the Fe triple-ζ valence (TZV)[57] basis set of (14s9p5d)/[10s8p3d]. A set of f functions was added to provide polarization ($\zeta = 1.663$).[58] For C and O the Dunning [5s, 3p][59] contraction of the (10s, 6p)[60] primitives were used as the TZV[57] basis set. One set of d functions was added to provide polarization for the C ($\zeta = 0.72$)[61] and O ($\zeta = 1.28$).[61] The quantum chemistry code GAMESS[62] was used, unless otherwise noted. The CO bond distance was fixed at 1.1283 Å for most PES, since previous work has shown that the positively charged Fe^+ ion causes little relaxation of the CO bond.[24] The geometries of the lowest lying quartet and sextet states were fully optimized including relaxation of the CO bond.

Most calculations presented in this work are based on fully-optimized reaction space (FORS)[63,64] MCSCF wavefunctions, also known as complete active space self-consistent field (CASSCF)[65–68] wavefunctions. The basic $FeCO^+$ wavefunction has 13 MCSCF core orbitals that are doubly occupied in all configurations and 11 orbitals with 13 electrons in the multi-configurational active space (13/11). The MCSCF active space includes the six valence 3d and 4s orbitals on Fe^+, σ donor lone pair orbital on CO, and CO π bonding and π^* anti-bonding orbitals. This active space allows for a proper treatment of the Fe^+ ion, carbon σ donation of the CO lone pair, and π backbonding into the CO π system. Reduced active spaces were appropriate in some instances and will be described below. The calculations on Fe^+ have a corresponding active space that includes the Fe^+ valence 3d and 4s orbitals. By carefully choosing orbitals, the MCSCF wavefunction was selectively converged to different spatial and spin symmetries. Dynamical correlation is usually necessary to obtain accurate energetics, therefore multi-configurational quasi-degenerate perturbation theory to second-order (MC-QDPT2)[51–53] was applied to the converged MCSCF wavefunction. The $FeCO^+$ MC-QDPT2 calculations correlated all molecular orbitals, except the 11 chemical core orbitals. In other words, the O lone pair and the CO σ bond orbitals were doubly occupied in the MCSCF wavefunction, but were correlated at the MC-QDPT2 level. The Fe^+ active space is the same in the MC-QDPT2 and MCSCF wavefunctions, with 9 chemical core orbitals.

The MC-QDPT2 method is not simply a multi-configurational extension of single-configuration Møller–Plesset (MP2)[69] perturbation theory, although MC-QDPT2 does include MP2 as a subset.[53] MC-QDPT2 is a multi-state and a multi-configurational perturbation method based on Van Vleck perturbation theory, while MP2 is based on Rayleigh–Schrödinger perturbation theory. The MC-QDPT2 approach facilitates an accurate treatment of both the ground state and excited states, with various space and spin symmetries (including simultaneously treating truly and nearly degenerate states correctly).[51,52] MC-QDPT2 is a perturb then diagonalize approach, in which the Hamiltonian is improved first with perturbation theory and then diagonalized to obtain the second-order energies.[70,71] The degenerate states ($^4\Delta$, $^4\Phi$, $^4\Pi$, $^6\Pi$, $^6\Delta$) are all treated using SA-MCSCF wavefunctions to properly account for their doubly degenerate nature. Since the states that are averaged are energetically equivalent, discontinuities[72] resulting from state-flipping do not appear in the SA-MCSCF PES.

Multi-reference second-order configuration interaction (MR-SOCI)[73,74] was also used to add correlation to selected MCSCF calculations. MR-SOCI involves single and double excitations out of the MCSCF active space, without reoptimizing the orbitals. This provides a variational method for adding second-order correlation effects to the wavefunction. MR-SOCI provides a variational check on the MC-QDPT2 wavefunction.

Some calculations presented are based on single-configuration wavefunctions. Coupled cluster theory including single and double replacements, with triples added perturbatively, has proven to be a powerful method for predicting the energetics of systems that can be treated with single-configuration wavefunctions. In this work, the CCSD(T)[75,76] method with the TZVP basis set has been used to investigate

Table 1 MCSCF NOON for Fe^+ with a TZVP basis set

	^6D	^4F
Fe 4s	1.000	0.003
Fe 3d	1.200	1.399

the $^4\Sigma^-$ $FeCO^+$ ground state. The results of these calculations are compared with those obtained using the multi-reference methods. To avoid spin-contamination, the zeroth-order wavefunction (ROHF) based formalism is used for the CCSD(T) calculations. The approach used is based on the Bartlett definition of RCCSD(T)[77] in which the triples are computed with contributions from both singles and doubles. This is the most common definition of open-shell triples although certainly not the only one.[78] The MOLPRO[79] *ab initio* package was used for most CCSD(T) calculations.

Spin–orbit coupling (SOC) has been shown to be important in the oxidative activation of H—H by FeO^+, therefore the effect of SOC on the predicted D_0 is undertaken.[91] Both one-electron and two-electron contributions to SOC are calculated.

III Fe^+

The Fe^+ ground and first excited states are known experimentally to be ^6D ($3d^64s^1$) and ^4F ($3d^74s^0$), respectively. The experimental splitting has been determined to be 5.35 kcal mol^{-1}.[27] SA-MCSCF calculations were performed to obtain the correct wavefunctions for the ^6D (five fold degenerate) and ^4F (seven fold degenerate) electronic states. MCSCF natural orbital occupation numbers (NOON) for both states are presented in Table 1 and the energy splittings at several levels of theory are given in Table 2. State averaging the wavefunction correctly gives all 3d orbitals the same NOON for each spin multiplicity. The poorly predicted splitting of 38.5 kcal mol^{-1} at the MCSCF level of theory is not surprising given the difficult nature of predicting the separation with *ab initio* methods.[80–83]

MR-SOCI and more efficient MC-QDPT2 calculations were carried out, to provide dynamic electron correlation in addition to the near degenerate correlation provided by the use of a multi-configurational wavefunction. The MC-QDPT2 results are closer to experiment than MCSCF, although this method does slightly overcorrect the MCSCF splitting. The MR-SOCI wavefunction has a larger absolute error than MC-QDPT2. The error for CCSD(T) lies between the MC-QDPT2 and MR-SOCI errors. Previous calculations on transition metal cations[84] suggest that additional polarization functions (*e.g.* g functions on Fe) may be necessary to obtain accurate

Table 2 Fe^+ relative energies with a TZVP basis set

State averaged	^4F–^6D Splitting/ kcal mol^{-1}	Error/ kcal mol^{-1}
Experiment	5.35	0.00
MCSCF	38.5	33.15
MCQDPT2	3.9	−1.42
MR-SOCI	12.6	7.29
MCSCF (g function added)	38.6	33.24
MCQDPT2 (g function added)	2.1	−3.24
MR-SOCI (g function added)	11.6	6.24
Single-reference CCSD(T)	10.0	4.64

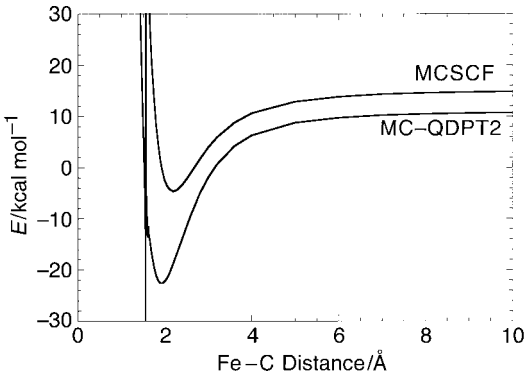

Fig. 1 $^4\Sigma^-$ $FeCO^+$ energy with a TZVP basis set and (13/11) active space.

atomic splitting. Adding a set of g functions ($\zeta = 1.7$) with the six orbital active space provides little improvement. Therefore g functions are not used in the $FeCO^+$ calculations.

IV $FeCo^+$

IVA Ground state PES

Initially the ground state PES for $^4\Sigma^-$ (as a function of the Fe–C distance) was calculated using the MCSCF/MC-QDPT2 method presented in Section II. For MCSCF wavefunctions, $^4\Sigma^-$ is found to be higher than the lowest sextet state (the lowest lying sextet state will be discussed in detail in Section IVB). With the addition of MC-QDPT2 dynamic correlation, the ground state for $FeCO^+$ is correctly found to be $^4\Sigma^-$. Just as in the Fe^+ calculations, correlation lowers the quartet states significantly more than the sextet states. Results are presented in Fig. 1, with the zero of energy defined by separated ^6D Fe^+ and ground state CO at each level of theory. The D_e with respect to ^4F Fe^+ is found to be 33.4 kcal mol^{-1} (at the low end of the experimental range) with an equilibrium distance of 1.93 Å. A discontinuity that appears at about 0.34 Å inside R_e is discussed in detail in Section V.

Close examination of the MCSCF and MC-QDPT2 potential energy curves reveals that the virtual 4s orbital on Fe^+ shifts onto CO as the complex dissociates. This results in a D_e that is too small (although the equilibrium geometry is valid). FORS-MCSCF is size-consistent, but size-consistency is only applicable if the active spaces in the separated Fe^+ and CO are the same as in the $Fe^+\cdots CO$ supermolecule. The shifting orbital resulted in a smaller active space on Fe^+ and a larger active space on CO in the supermolecule. Variational methods such as MCSCF can correct for poorly chosen orbitals and lower the energy, but perturbative methods such as MC-QDPT2 require a well-balanced active space to be reliable. Therefore this orbital was removed from the $^4\Sigma^-$ MCSCF active space. The results with the (13/10) active space are presented in Fig. 2; the D_e is found to be 36.5 kcal mol^{-1} with

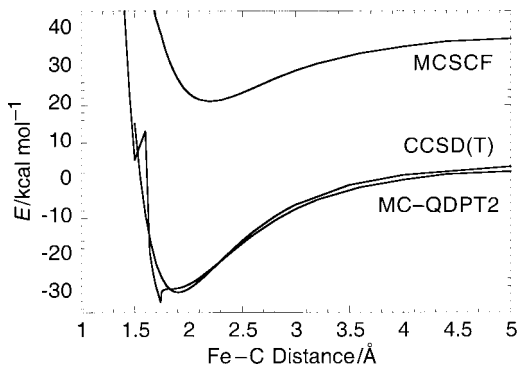

Fig. 2 $^4\Sigma^-$ $FeCO^+$ energy with a TZVP basis set with CCSD(T) and MCSCF (13/10).

Table 3 IR frequencies (cm^{-1}) and intensities [D^2/(amu Å^2)] for $FeCO^+$ $^4\Sigma^-$

	$FeCo^-$ exp.	FeCO exp.	$FeCO^+$ exp.	$FeCO^+$ MP2	$FeCO^+$ B3LYP	$FeCO^+$ CCSD(T)	$FeCO^+$ $^6\Delta$ MC-QDPT2
Fe–C stretch	565 ± 10[b] 740[a]	530 ± 10[b]	—	405[c]	423[c]	435 (2.79)	206 (1.04)
C–O stretch	1980[a]	1950 ± 10[b] 1815[a]	—	2153[c]	2225[c]	1830 (5.06)	1857 (0.066)
Linear bend	230 ± 40[b]	330 ± 50[b]	—	321[c]	319[c]	313 (small)	172 (0.156)

[a] Ref. 89. [b] Ref. 12. [c] Ref. 25.

respect to ^{4}F Fe^+ (within the experimental range). The equilibrium Fe–CO distance is 1.75 Å. Unfortunately, this (13/10) $^4\Sigma^-$ PES has a discontinuity near the MC-QDPT2 minimum, making the geometry suspect. Similar behavior is found using the multi-reference CI wavefunction. This discontinuity is discussed in detail in Appendix A.

Since the largest natural orbital occupation number in the virtual space of the $^4\Sigma^-$ state is less than 0.1, it is reasonable to use single-reference CCSD(T) for the ground state.[85–87] Thus, although this method does have a lower quality zeroth order wavefunction (ROHF) than MC-QDPT2 (MCSCF), the final results should be accurate. There are no unusual features in the CCSD(T) PES as shown in Fig. 2. By fitting the points on the CCSD(T) PES, the D_e with respect to ^{4}F Fe^+ is found to be 35.0 kcal mol^{-1} with an equilibrium Fe–CO distance fixed at 1.1283 Å. This D_e is in good agreement with the experimental results and close to the MC-QDPT2 D_e, despite the problems encountered with that method.

The geometry of the $^4\Sigma^-$ state was optimized at the CCSD(T) level of theory. The molecule was not assumed to be linear, although all attempts at bending the $FeCO^+$ increased the energy at the MCSCF, MC-QDPT2, and CCSD(T) levels of theory. One cannot assume that excited electronic states are linear, particularly since bent excited and ground states are not uncommon for third row metal carbonyls.[88] The minimum energy CCSD(T) geometry is $C_{\infty v}$ with a Fe^+–CO distance of 1.905 Å and a CO bond distance of 1.133 Å. The CO bond did not relax significantly during interaction with Fe^+, because there is little charge transfer into the CO bond region. The CCSD(T) D_e for dissociation of $^4\Sigma^-$ $FeCO^+$ to ^{4}F Fe^+ is 35.1 kcal mol^{-1}. Note that only 0.1 kcal mol^{-1} is gained by allowing the CO bond length to relax. Based on the experimental quartet–sextet splitting of 5.35 kcal mol^{-1}, the CCSD(T) D_e for dissociation of $^4\Sigma^-$ $FeCO^+$ to ^{6}D Fe^+ should be 29.7 kcal mol^{-1}.

A numerical CCSD(T) hessian was calculated for the $^4\Sigma^-$ state. A double differences approach was used to minimize the possibility of numerical error (see Appendix B). The frequencies are not scaled, because CCSD(T) should give high quality results. The frequencies and associated intensities are compared with experiment[12,89] and previously calculated[25] spectra in Table 3. Intensities are based on the ROHF dipole derivative tensor and the CCSD(T) hessian. The CCSD(T) predicted CO stretch is smaller than the MP2 and B3LYP frequencies. If the experimental values for $FeCO^-$ and FeCO are a valid guide, then the CCSD(T) frequencies are not unreasonable. A vibrational analysis of the normal modes leads to a zero-point energy (ZPE) of 4.13 kcal mol^{-1}. The CO molecule has a ZPE of 3.18 kcal mol^{-1}, calculated using closed-shell CCSD(T) with ACESII.[90] This results in a net ZPE correction of 0.95 kcal mol^{-1} for the $FeCO^+$ complex. Therefore, the D_0 for dissociation to ^{4}F Fe^+ is 34.2 kcal mol^{-1}. The D_0 for dissociation to ^{6}D Fe^+ is 28.8 kcal mol^{-1}, at the low end of the experimental range presented in Section I.

IVB Excited states

The $^6\Sigma^+$, $^6\Delta$, $^6\Pi$, and $^4\Delta$ states were each separately optimized. Degenerate states were state averaged (SA-MCSCF) over both components to preserve orbital and hence state degeneracy. MC-QDPT2 was applied as a perturbation to add dynamical correlation to obtain reliable energetics and geometries, with two roots included in the treatment when the state was degenerate. The (13/11) MCSCF active space presented in Section II was used for the $^6\Delta$ and $^6\Pi$ states.

When a (13/11) active space is used for the $^4\Delta$ state, the virtual 4s orbital becomes a CO virtual orbital as the complex dissociates, resulting in improper energetics, similarly to the $^4\Sigma^-$ state in Section IVA. Thus, this CO orbital was removed from the $^4\Delta$ MCSCF active space, yielding a (13/10) active space. This removal does not reduce the effective size of the active space, because neither this orbital nor the 4s is significantly populated in the quartet states. For Fe^+ ion, removing the 4s orbital raises the MCSCF energy 0.8 kcal mol^{-1}, and lowers the MC-QDPT2 energy 0.04 kcal mol^{-1}.

For the $^6\Sigma^+$ and the $^4\Delta$ states, the 3d σ orbital should be doubly occupied in all configurations due to spatial and spin symmetry. Therefore, the MCSCF active space for the $^6\Sigma^+$ and the $^4\Delta$ states was reduced by one orbital to force the 3d σ orbital to be doubly occupied in all configurations. This yields (11/10) and (11/9) active spaces, respectively, for the two states. This reduction does not reduce the effective size of the active space relative to the other states, because removing an orbital that is doubly occupied in all configurations does not shrink the effective active space. These reduced, but properly dissociating, active spaces are then used to calculate MCSCF and MC-QDPT2 energies for the $^6\Sigma^+$ and the $^4\Delta$ states. The energies of the $^4\Delta$ (11/9), $^6\Sigma^+$ (11/10), $^6\Pi$ (13/11), and $^6\Delta$ (13/11) states are presented as a function of the Fe–C distance in Fig. 3 and 4 for MCSCF and MC-QDPT2, respectively. At the higher level of theory, the potential energy minimum of the $^4\Delta$ state is well below that of the others and has a shorter Fe–C equilibrium distance.

Since the $^4\Pi$ and $^4\Phi$ states could not be individually optimized, an additional set of SA-MCSCF calculations were performed in which all sextet states and all quartet states were state-averaged (separately for each multiplicity) to obtain energies for all 12 states with the (13/11) active space. The results of these calculations are shown in Fig. 5 and 6, for MCSCF and MC-QDPT2 respectively. These calculations cannot be used directly to obtain D_e values or geometries, because the state averaging gives geometries and energies that depend on all the states. The curves in Fig. 6 do suggest that the $^4\Pi$ and $^4\Phi$ states should lie between the $^4\Delta$ and $^4\Sigma^-$ states. Therefore the ranges that the D_e and equilibrium distances must fall into are known for $^4\Pi$ and $^4\Phi$, even if exact values are not. All states are found to be bound in all of the calculations. Therefore even if the $FeCO^+$ complex is in a low lying excited state when it initially forms from Fe^+ and CO, it will most likely be a bound state.

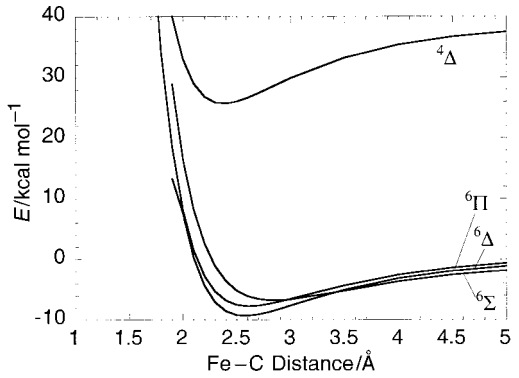

Fig. 3 $FeCO^+$ excited state MCSCF energies with a TZVP basis set.

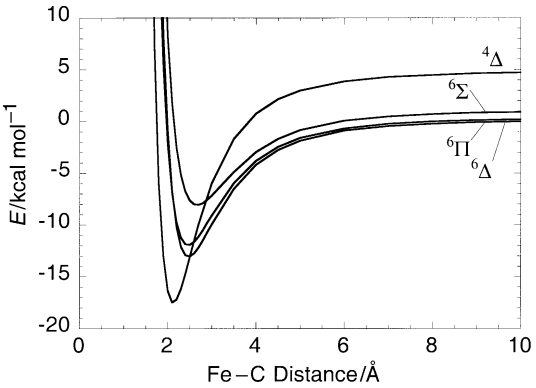

Fig. 4 $FeCO^+$ excited state MC-QDPT2 energies with a TZVP basis set.

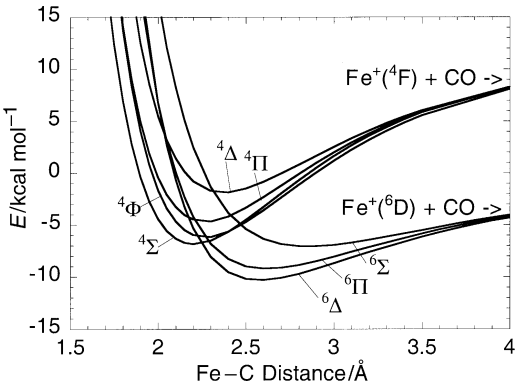

Fig. 5 $FeCO^+$ MCSCF energy (all states averaged).

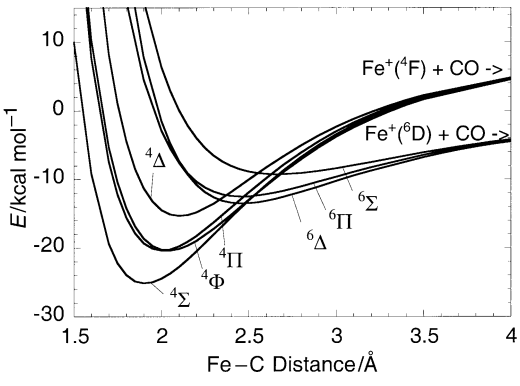

Fig. 6 $FeCO^+$ MC-QDPT2 energy (all states averaged).

Table 4 MC-QDPT2 equilibrium distances and dissociation energies for $FeCO^+$ relative to ^6D Fe^+ and CO

	Fe–CO distance/Å	D_e/kcal/mol^{-1}
$^4\Sigma^-$ CCSD(T)	1.91	29.7
$^4\Sigma^-$ (13/11)	1.93	22.7
$^4\Sigma^-$ (13/10)	1.75	32.3
$^4\Delta$ (11/9)	2.1	17.5
$^6\Delta$ (13/11)	2.5	12.7
$^6\Pi$ (13/11)	2.5	11.9
$^6\Sigma^+$ (11/10)	2.7	8.1

Dissociation energies for $FeCO^+$ excited states relative to the ^6D ground state were calculated by assuming a fixed CO distance and a linear $FeCO^+$ at the MC-QDPT2 level. The properly dissociating active spaces presented above in Fig. 4 were used. These results along with the corresponding Fe^+–CO equilibrium distances are presented in Table 4. As the equilibrium distance increases, the calculated D_e decreases, as one would expect.

MCSCF NOON are presented for all states at the MC-QDPT2 equilibrium geometries in Table 5. For states with active spaces smaller than the original (13/11), the orbitals not in the active space are designated in Table 5 as integer NOON with no trailing zeros. The quartet states are found to have an empty Fe 4s orbital while the sextet states have a singly occupied Fe 4s orbital. This difference allows the quartet $FeCO^+$ states to more readily accept electron density from other molecules. This explains the experimentally observed greater reactivity of $FeCO^+$ versus Fe^+. All of the quartet states are found to be lower in energy than all of the sextet states. Therefore, the lowest excited states are likely to show this enhanced reactivity.

Because $^6\Delta$ is the lowest sextet state, a numerical MC-QDPT2 hessian was calculated using finite differences. The large basis MP2 scaling factor is 0.94–1.02 depending on whether one is fitting ω, ZPE, $\Delta H_{vib}(T)$, $1/\omega$, or $S_{vib}(T)$.[92] MC-QDPT2 should calculate frequencies more accurately than MP2, so a scaling factor of 1.0 was assumed. Intensities presented are based on the MCSCF dipole derivative tensor and the MC-QDPT2 hessian. These frequencies and intensities are presented in Table 3. The $^6\Delta$ $FeCO^+$ ZPE is 3.44 kcal mol^{-1} and the CO ZPE is 3.02 kcal mol^{-1}. The net $^6\Delta$ $FeCO^+$ ZPE is 0.42 kcal mol^{-1}, resulting in a $^6\Delta$ D_0 of 12.3 kcal mol^{-1}.

IVC The effect of spin–orbit coupling

Since the Fe^+ states have many unpaired electrons, it is of interest to explore the effects of spin–orbit splitting on the predicted dissociation energies. Both one-electron and two-electron contributions to the spin–orbit coupling (SOC) have therefore been calculated as a perturbation to the quartet and

Table 5 MCSCF NOON for $FeCO^+$ with a TZVP basis set

	$^4\Sigma^-$	$^4\Delta$	$^6\Delta$	$^6\Pi$	$^6\Sigma^+$
CO π^*	0.083	0.059	0.059	0.059	0.059
Fe 4s σ	0	0	1.000	1.000	1.000
Fe 3d δ	1.028	1.500	1.500	1.000	1.000
Fe 3d π	1.931	1.000	1.000	1.500	1.000
Fe 3d σ	1.004	2	1.000	1.000	2
CO π	1.963	1.945	1.945	1.956	1.946
CO σ	1.986	1.981	1.991	1.990	1.990

sextet MCSCF wavefunctions, using a method recently developed by Federov and co-workers.[93] In Fe^+, the ^6D state energy increases by 0.4 kcal mol^{-1} relative to the ^4F. For $FeCO^+$ at the CCSD(T) equilibrium geometry, introduction of the spin–orbit interaction raises the $^6\Delta$ state by 1.2 kcal mol^{-1} relative to the $^4\Sigma^-$. So, SOC has only a small ($\leqslant$1.6 kcal mol^{-1}) effect on the predicted dissociation energies. This is consistent with previous calculations on $FeO^+ + H_2$.[94]

V Problems with multi-reference perturbation theory

Careful analysis of the (13/10) $^4\Sigma^-$ PES reveals that a discontinuity is present on the MC-QDPT2 surface at 1.560516 Å. Failures of single-refrence Møller–Plesset have been reported in the literature, even for a single Ne atom.[95] There are reports of similar problems within the multi-reference CASPT2 extension of MP2.[96,97] The PES of the divergent state is illustrated in Fig. 7. The energies plotted are total energies with the zero of energy defined as MC-QDPT2 separated Fe^+ and CO. The MC-QDPT2 "correction" to the MCSCF energy is positive on one side of the discontinuity and negative on the other side. The energy difference between R(Fe–C) = 1.560515 Å and 1.560516 Å is 376 E_h for MC-QDPT2 and only 0.0003 kcal mol^{-1} for MCSCF. This discontinuity is particularly troubling because such problems are usually expected to occur in excited state calculations. The MC-QDPT2 PES is smooth elsewhere, so the discontinuity is localized. Fortunately, the discontinuity is not near the minimum energy point or dissociation, so predicted properties are not corrupted.

The choice of perturbation theory does effect the energies calculated: Møller–Plesset (MP) and Epstein–Nesbet (EN) partition differently and achieve perturbation expansions that behave differently.[98,99] The MC-QDPT2 calculation is performed on the canonicalized Fock orbitals, because perturbation theory requires orbital energies. Canonicalization is a rotation within the active space, so the MCSCF wavefunction is unchanged. For a perturbation expansion to be valid, the zeroth-order wavefunction Ψ^0 must be a close approximation to the exact wavefunction Ψ. In the single-state case of $^4\Sigma^-$, the weight of the reference function in the first-order wavefunction is defined by eqn. (1):

$$W = \frac{\langle \Psi^0 | \Psi^0 \rangle}{\langle \Psi^0 + \Psi^1 | \Psi^0 + \Psi^1 \rangle} \quad (1)$$

where Ψ^1 is the first-order correction to the wavefunction and $\Psi = \Psi^0 + \Psi^1 + \Psi^2 + \Psi^3 + \cdots$. Therefore, $\Psi^0 + \Psi^1$ is the first-order wavefunction. Ψ^0 and Ψ^1 are orthogonal and Ψ^0 is normalized, so eqn. (1) simplifies with a little mathematical manipulation to eqn. (2).

$$W = \frac{1}{1 + \langle \Psi^1 | \Psi^1 \rangle} \quad (2)$$

The weight W is nearly 0% at the discontinuity. Thus, this wavefunction is a truly divergent case at second-order. Several values of W are plotted in Fig. 7. The weight is >89% from 1.7 Å to dissociation and >87% for R(Fe–C) $\leqslant$ 1.4 Å. Clearly, even though the perturbation expansion is failing for the $^4\Sigma^-$ PES, the MC-QDPT2 method is surprisingly robust, giving reasonable energies for values of W as small as 25%.

The MCSCF wavefunction was examined in an effort to obtain some theoretical insight. When orbitals cross, the nature of a state can shift suddenly. The number of degenerate molecular orbitals was not different at the discontinuity, so an orbital crossing (including virtuals) was not causing the divergence. MCSCF NOON provide insight into the multi-reference nature of a wavefunction; however the NOON are smoothly varying in the region of the discontinuity. The largest variance anywhere on the PES from single-reference values of 0, 1, and 2 is only 0.1598, and this is at the unbound geometry.

The gap between the highest energy MCSCF active orbital and the lowest non-active virtual orbital is 62 kcal mol^{-1}. Thus, this divergence was not caused by a low lying orbital that should have been included in the MCSCF active space. Using a full configuration interaction (CI) within the MCSCF active space, the next highest state is found to be 27.9 kcal mol^{-1} higher. Therefore a low lying excited state is also not the underlying cause. A variational second-order approach was utilized to further examine the validity of the underlying MCSCF wavefunction. An internally contracted multi-reference second-order CI[100,101](SOCI) produces energies that are reasonable and smooth in the region of the divergence. This suggests that the origin of the MC-QDPT2 divergence does not lie in the MCSCF orbitals, but rather within the perturbation expansion itself.

MC-QDPT2 divergences can be artificially avoided. One way to avoid the divergence is to change the reference function. A logical choice is to replace the canonical Fock orbitals with the natural orbitals.[102] These orbitals diagonalize the first-order density matrix rather than the generalized Fock matrix. The MC-QDPT2 energy is not invariant with respect to orbital rotations within the active space, unlike the FORS-MCSCF energy. Using natural orbitals results in different orbital energies, and the choice of orbital energies affects convergence of the perturbation expansion.[103] The validity of such a substitution is not known, particularly since orbital energies are not as well-defined for natural orbitals. A configuration state function (CSF) selection scheme could be utilized, in which the CSFs that contribute little to the MCSCF wavefunction are not used in the perturbation step.[104] However, this is an arbitrary restriction on the MC-QDPT2 calculation, and this restriction might introduce problems of its own. A chemically important CSF might be left out of the MC-QDPT2 calculation, resulting in spurious results. A third approach is to change the active spaces. Several attempts to vary the MCSCF and MC-QDPT2 active spaces were undertaken and although the divergence shifted to other distances, it usually did not disappear. These three modifications have the downside of changing the nature of the perturbation method, and therefore all calculations would have to be done using these modifications with no guarantee of not introducing another divergence or other problem.

The cause of these divergences may be understood by examining mathematics of expansions. The Hamiltonian is expanded in the space of perturbation parameter λ about $\lambda = 0$ and evaluated at $\lambda = 1$. In the case of MC-QDPT, $\lambda = 0$

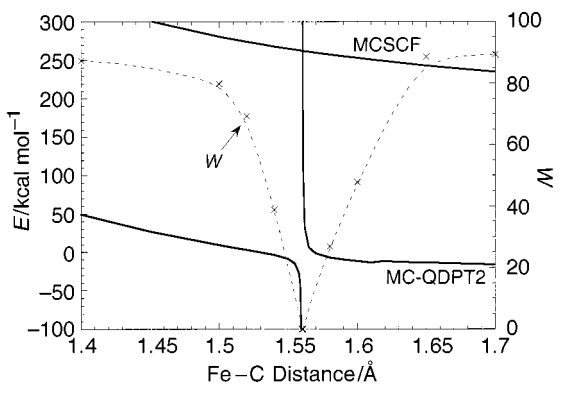

Fig. 7 MC-QDPT2 divergence in $FeCO^+$ (13/11) PES. E = energy, W = weight of reference wavefunction in MC-QDPT2 wavefunction.

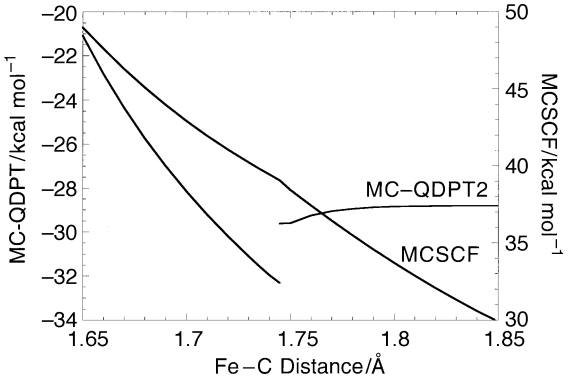

Fig. A1 MCSCF discontinuity in $^4\Sigma^-$ $FeCO^+$ (13/10) PES.

corresponds to the MCSCF reference wavefunction and $\lambda = 1$ corresponds to the MC-QDPT wavefunction. As λ goes from 0 to 1, the correlation is turned on. If the perturbation expansion converges, the MC-QDPT wavefunction is the exact wavefunction. MC-QDPT2 truncates the expansion at the second-order terms. Singularities can appear within the λ space. The singularity nearest to $\lambda = 0$ limits the radius of convergence. The expansion is valid for all λ that are closer to $\lambda = 0$ than this singularity. For λs outside the radius of convergence, it is possible for the perturbation series to converge, but often to the wrong number.[105] This problem is not limited to perturbation expansions; divergences limit the usefulness of all expansions, such as Taylor series.[106] Singularities are not limited to real values of λ and therefore predicting or interpreting these problems is difficult.

VI Conclusions

Fe^+ and its complexes such as $FeCO^+$ are interesting due to their chemical reactivity as catalysts. CO is of particular interest, because it is especially effective in stabilizing transition metals. The addition of CO to Fe^+ changes the reactivity significantly, because the ground state changes from a sextet to a quartet upon formation of the $FeCO^+$ complex. This change in spin results from a change in the 4s orbital occupation from one to zero. The three low lying excited states are also quartets, therefore this enhanced reactivity is probably present in these lowest excited states. Results from a careful study reveal that uncorrelated wavefunctions such as MCSCF fail to properly handle this shift from sextet to quartet. MCSCF predicts that the sextet is always lower than the quartet in energy. Dynamical correlation is found to be necessary to achieve proper energetics. In the present work, dynamic correlation is obtained with both MC-QDPT2 and single-reference ROHF based CCSD(T). These two methods predict dissociation energies for the $^4\Sigma^-$ ground state that are comparable to the experimental values ($D_0 = 28.8$–37.7 kcal mol^{-1}). With the addition of zero-point corrections, the CCSD(T) predicted D_0 is found to be 28.8 kcal mol^{-1}. The MC-QDPT2 D_e is found to be 32.3 kcal mol^{-1}. The lowest lying sextet state, $^6\Delta$, is predicted by MC-QDPT2 to have a D_0 of 12.3 kcal mol^{-1}. Therefore, $FeCO^+$ gains 16.5 kcal mol^{-1} in energy when it changes spin states. The $^6\Delta$ and $^4\Sigma^-$ states can be differentiated experimentally by their IR spectra. The CO stretch frequencies for the $^6\Delta$ and $^4\Sigma^-$ are very similar, but the $^6\Delta$ intensity is very small. The Fe–C stretch frequencies differ by 229 cm^{-1}. In both states the linear bend has the smallest IR intensity. During the analysis of the $FeCO^+$ system, difficulties at several levels of theory were discovered and analyzed.

Acknowledgements

This work was supported in part by grants from the Air Force Office of Scientific Research (F49-620-97-1-0522) and by the Ames Laboratory, US-DOE. The authors would like to thank Dmitri Fedorov, Dr Mike Schmidt and Dr Cheuk Ng for many enlightening conversations. The authors would also like to thank Dmitri Fedorov for access to his spin–orbit coupling code.

Appendix A A MCSCF discontinuity

The $^4\Sigma^-$ (13/10) MCSCF curve has a discontinuity, which is presented in Fig. A1. This jump is caused by a sudden change in the CO π^* NOON from 0.09 to 0.06. This change causes a change in the shape in the MCSCF curve and a break in the MC-QDPT2 curve. The NOON change occurs near the MC-QDPT2 minimum, so optimizing the geometry is not possible. This bump was investigated with SOCI based on the MCSCF reference[107,108] using MOLPRO. This variational method gives a similarly discontinuous PES. This means that the underlying MCSCF wavefunction is pathological or incorrect; therefore, this is not a MC-QDPT2 divergence as discussed in Section V. A full CI within the FORS space was done, and no low lying states were found on either side of the split, and none of the lowest states were $^4\Sigma^-$ states. Removal of the π^* orbital from the MCSCF active space solved the problem; this solution removes all virtual orbitals from the MCSCF active space, leaving a predominantly single-reference wavefunction. An effort to incrementally improve the active space by moving core orbitals into the active space failed to remove the discontinuity.

Appendix B The calculation of a hessian using a fully numerical approach

Because $FeCO^+$ is a small linear molecule, the hessian is much simpler to calculate in internal coordinates. The two bending terms are degenerate and therefore only one must be calculated. Because $E(\theta)$ is symmetrical about the linear bend θ, $(\partial E/\partial\theta)_{\theta=180^\circ}$ vanishes. Therefore $(\partial^2 E/\partial S\partial\theta)_{\theta=180^\circ}$ must also vanish, where S is a bond stretch. Therefore in linear $FeCO^+$, the bend–stretch cross-terms vanish. The two stretches (Fe–C and C–O) are not independent, so two pure terms and two equal cross-terms must be calculated. S_1, S_2 = distances and L, K = offset are used in the derivation. Offsets

Table B1 Fully numerical $^4\Sigma^-$ hessian in internal coordinates

	FeC stretch	Co stretch	FeCo bend	FeCo bend
FeC stretch	1.239 E_h a_0^{-2}	0.0316 E_h a_0^{-2}	0.0000	0.0000
CO stretch	0.0316 E_h a_0^{-2}	0.0943 E_h a_0^{-2}	0.0000	0.0000
FeCO linear bend	0.0000	0.0000	0.0604 E_h rad^{-2}	0.0000
FeCO linear bend	0.0000	0.0000	0.0000	0.0604 E_h rad^{-2}

of 0.02, 0.01 and 0.005 Å and 1, 2, 3, 4, 5 and 6° were averaged to reduce the possiblity of numerical error. The stretch cross-term is:

$$\left.\frac{\partial^2 E(S_1, S_2)}{\partial S_1 \partial S_2}\right|_{S_1=S_2=0} = \frac{[E(L, L) + E(-L, -L)] - [E(L, -L) + E(-L, L)]}{4L^2} \quad \text{(C1)}$$

Stretch terms, for which $S_1 = S_2$, are:

$$\left.\frac{\partial^2 E(S_1)}{\partial S_1 \partial S_1}\right|_{S_1=0} = \frac{[E(K) + E(-K)] - [2E(0)]}{K^2} \quad \text{with } K = 2L \quad \text{(C2)}$$

Bending terms, for which $E(\theta) = E(-\theta)$, are:

$$\left.\frac{\partial^2 E(\theta)}{\partial\theta\ \partial\theta}\right|_{\theta=0} = \frac{[2E(K)] - [2E(0)]}{K^2} \quad \text{(C3)}$$

The resulting hessian is presented in Table B1.[109]

References

1 J. E. Ellis, *Adv. Organomet. Chem.*, 1990, **31**, 1.
2 *Catalytic Act. Carbon Monoxide Symp., ACS Symp. Ser.*, ed. P. C. Ford, ACS, Washington DC, 1981, **152**.
3 P. K. Hurlburt, J. J. Rack, J. S. Luck, S. F. Dec, J. D. Webb, O. P. Anderson and S. H. Strauss, *J. Am. Chem. Soc.*, 1994, **116**, 10003 and references therein.
4 Chemical Abstracts Service Online.
5 G. Henrici-Olivé and S. Olivé, *The Chemistry of Catalyzed Hydrogenation of Carbon Monoxide*, Springer-Verlag, Berlin, 1984, and references therein.
6 X. W. Fan, X. J. Chen, S. J. Zhou, Y. Zheng, C. E. Brion, R. Frey and E. R. Davidson, *Chem. Phys. Lett.*, 1997, **276**, 346.
7 F. Meyer, Y-M. Chen and P. B. Armentrout, *J. Am. Chem. Soc.*, 1995, **117**, 4071.
8 M. R. Sievers and P. B. Armentrout, *J. Phys. Chem.*, 1995, **99**, 8135.
9 P. Mourgues and G. Ohanessian, *Rapid Commun. Mass. Spectrom.*, 1995, **9**, 1201.
10 Y-J. C-L. Liao and C. Y. Ng, *J. Chem. Phys.*, 1997, **107**, 4527.
11 L. S. Sunderlin, D. Wang and R. R. Squires, *J. Am. Chem. Soc.*, 1992, **114**, 2788.
12 P. W. Villalta and D. G. Leopold, *J. Chem. Phys.*, 1993, **98**, 7730.
13 S. Goebel, C. L. Haynes, F. A. Khan and P. B. Armentrout, *J. Am. Chem. Soc.*, 1995, **117**, 6994.
14 K. Norwood, A. Ali, G. D. Flesch and C. Y. Ng, *J. Am. Chem. Soc.*, 1990, **112**, 7508.
15 M. Sablier, H. Mestdagh and C. Rolando, *J. Phys. Chem.*, 1994, **98**, 8320.
16 J. H. Butler, J. W. Elkins, B. D. Hall, S. O. Cummings and S. A. Montzka, *Nature* (*London*), 1992, **359**, 403.
17 P. B. Armentrout and B. J. Tjelta, *Organometallics*, 1997, **16**, 5372.
18 A. Ricca and C. W. Bauschlicher, *J. Phys. Chem.*, 1995, **99**, 9003.
19 D. Schröder and H. Schwarz, *J. Organomet. Chem.*, 1995, **504**, 123.
20 B. L. Tjelta and P. B. Armentrout, *J. Am. Chem. Soc.*, 1996, **118**, 9652.
21 L. Bañares, T. Baumert, M. Bergt, B. Kiefer and G. Gerber, *Chem. Phys. Lett.*, 1997, **267**, 141.
22 B. K. Venkararaman, H. Bandukwalla, Z. Zhang and M. Vernon, *J. Chem. Phys.*, 1989, **90**, 5510.
23 T. Majima, *Coord Chem. Rev.*, 1994, **132**, 141.
24 M. Castro, D. R. Salahub and R. Fourner, *J. Chem. Phys.*, 1994, **100**, 8233.
25 A. Ricca and C. W. Bauschlicher, *J. Phys. Chem.*, 1994, **98**, 12899.
26 M. N. Glukhovtsev, R. D. Bach and C. Nagel, *J. Phys. Chem. A*, 1997, **101**, 316.
27 J. Sugar and C. Corioliss, *J. Phys. Chem. Ref. Data, Suppl. 2*, 1985, **14**, 407.
28 D. Schröder, A. Fiedler and H. Schwarz, *Int. J. Mass. Spectrom. Ion Processes*, 1994, **134**, 239.
29 B. L. Tjelta and P. B. Armentrout, *J. Phys. Chem.*, 1997, **101**, 2064.
30 L. Capron, W. Y. Feng, C. Lifshitz, B. L. Tjelta and P. B. Armentrout, *J. Phys. Chem.*, 1996, **100**, 16571.
31 V. Baranov and D. K. Bohm, *Int. J. Mass Spectrom. Ion Processes*, 1996, **154**, 71.
32 R. H. Schultz, K. C. Crellin and P. B. Armentrout, *J. Am. Chem. Soc.*, 1991, **113**, 8590.
33 C. J. Carpenter, P. A. M. van Koppen and M. T. Bowers, *J. Am. Chem. Soc.*, 1995, **117**, 10976.
34 K. Norwood, J-H. Guo, G. Lou and C. Y. Ng, *J. Chem. Phys.*, 1989, **90**, 6026.
35 K. Norwood, J-H. Guo, G. Lou and C. Y. Ng, *Chem. Phys.*, 1989, **129**, 109.
36 K. Norwood, J-H. Guo and C. Y. Ng, *J. Chem. Phys.*, 1989, **90**, 2995.
37 K. Norwood and C. Y. Ng, *Chem. Phys. Lett.*, 1989, **156**, 145.
38 R. H. Hertwig and W. Koch, *Chem. Phys. Lett.*, 1997, **268**, 345.
39 A. Ricca and C. W. Bauschlicher, *Theor. Chim. Acta*, 1995, **92**, 123.
40 P. E. M. Siegbahn, in *Advances in Chemical Physics*, **XCIII**, ed. I. Prigogine and S. A. Rice, John Wiley & Sons, Inc., 1996.
41 A. Ricca and C. W. Bauschlicher, *J. Phys. Chem.*, 1995, **99**, 5922.
42 C. Adamo and F. Lelj, *Chem. Phys. Lett.*, 1995, **246**, 463; *J. Chem. Phys.*, 1995, **103**, 10605.
43 B. J. Persson, B. O. Roos and K. Pierloot, *J. Chem. Phys.*, 1994, **101**, 6810.
44 M. W. Schmidt and M. S. Gordon, *Annu. Rev. Phys. Chem.*, 1998, **49**, 233.
45 J. Andzelm, N. Russo and D. Salahub, *J. Chem. Phys.*, 1987, **87**, 6562.
46 S. G. Wang and W. H. E. Schwarz, *J. Chem. Phys.*, 1996, **105**, 4641.
47 W. Weinert and J. W. Davenport, *Phys. Rev. B*, 1992, **45**, 13709.
48 R. W. Warren and B. I. Dunlap, *Chem. Phys. Lett.*, 1996, **262**, 384.
49 S. Grimme, *Chem. Phys. Lett.*, 1996, **259**, 128.
50 B. O. Roos, in *Lecture Notes in Quantum Chemistry*, ed. B. O. Roos, Springer-Verlag, Berlin, 1994, vol. 58, 177–254.
51 H. Nakano, *J. Chem. Phys.*, 1993, **99**, 7983.
52 H. Nakano, *Chem. Phys. Lett.*, 1993, **207**, 372.
53 H. Nakano, K. Hirao and M. S. Gordon, *J. Chem. Phys.*, 1998, **108**, 5660.
54 R. D. Bartlett, in *Modern Electronic Structure Theory. I.*, ed. D. R. Yarkony, World Scientific, Singapore, 1995, p. 1047.
55 A. J. H. Wachters, *J. Chem. Phys.*, 1970, **52**, 1033.
56 A. K. Rappé, T. A. Smedley and W. A. Goddard III, *J. Phys. Chem.*, 1981, **85**, 2607.
57 Selected by GBASIS = TZV keyword in GAMESS.
58 K. R. Glaesemann and M. S. Gordon, unpublished.
59 T. H. Dunning, *J. Chem. Phys.*, 1971, **55**, 716.
60 S. Huzignaga, *J. Chem. Phys.*, 1965, **42**, 1293.
61 Selected by POLAR = HONDO7 keyword in GAMESS. This is the default polarization for the TZV basis set in GAMESS.
62 GAMESS (General Atomic and Molecular Electronic Structure System): M. W. Schmidt, K. K. Baldridge, J. A. Boatz, S. T. Elbert, M. S. Gordon, J. H. Jensen, S. Koseki, N. Matsunaga, K. A. Nguyen, S. Su, T. L. Windus, M. Dupuis and J. A. Montgomery, Jr., *J. Comput. Chem.*, 1993, **14**, 1347; http://www.msg.ameslab.gov/GAMESS/GAMESS.html.
63 K. Ruedenberg and K. R. Sundberg, in *Quantum Science*, ed. J. L. Calais, O. Goscinski, J. Linderberg and Y. Ohrn, Plenum, NY, 1976, p. 505.
64 L. M. Cheung, K. R. Sundberg and K. Ruedenberg, *Int. J. Quantum Chem.*, 1979, **16**, 1103.
65 B. O. Roos, in *Advances in Chemical Physics*, ed. K. P. lawley, Wiley Interscience, New York, 1987, vol. 69, p. 339.
66 P. E. Siegbahn, A. Heiberg, B. O. Roos and B. Levy, *Phys. Scr.*, 1980, **21**, 323.
67 B. O. Roos, P. R. Taylor and P. E. Siegbahn, *Chem. Phys.*, 1980, **48**, 157.
68 B. O. Roos, *Int. J. Quantum Chem.*, 1980, **S14**, 175.
69 J. Pople, J. S. Binkley and R. Seeger, *Int. J. Quantum Chem., Quantum Chem. Symp.*, 1976, **10**, 1.
70 P. M. Kozlowski and E. R. Davidson, *J. Chem. Phys.*, 1994, **100**, 3672.
71 J. J. W. McDouall, K. Peasley and M. A. Robb, *Chem. Phys. Lett.*, 1988, **148**, 183.
72 A. Zaitsevskii and J-P. Malrieu, *Chem. Phys. Lett.*, 1994, **228**, 458.

73 B. Brooks and H. F. Schaefer, *J. Chem. Phys.*, 1979, **70**, 5092.
74 T. Helgaker, J. Gauss, P. Jørgensen and J. Olsen, *J. Chem. Phys.*, 1997, **106**, 6430.
75 G. E. Scuseria, C. L. Janssen and H. F. Schaefer III, *J. Chem. Phys.*, 1988, **89**, 7382.
76 J. F. Stanton, *Chem. Phys. Lett.*, 1997, **281**, 130.
77 J. D. Watts, J. Gauss and R. J. Bartlett, *J. Chem. Phys.*, 1993, **98**, 8718.
78 M. J. O. Deegan and Peter J. Knowles, *Chem. Phys. Lett.*, 1994, **227**, 321.
79 MOLPRO (a package of *ab initio* programs): H-J. Werner and P. J. Knowles, with contributions from J. Almlöf, R. D. Amos, M. J. O. Deegan, S. T. Elbert, C. Hampel, W. Meyer, K. Peterson, R. Pitzer, A. J. Stone, P. R. Taylor and R. Lindh.
80 J. Moc and M. S. Gordon, *Organometallics*, 1997, **16**, 27; www.tc.bham.ac.uk/molpro.html.
81 D. G. Musaev and K. J. Morokuma, *J. Chem. Phys.*, 1994, **101**, 10697.
82 L. F. Pacios and P. G. Calzada, *Int. J. Quantum Chem.*, 1988, **34**, 267.
83 T. Ziegler and J. Li, *Can. J. Chem.*, 1994, **72**, 783.
84 T. Taketsuga and M. S. Gordon, *J. Chem. Phys.*, 1997, **106**, 8504.
85 J. M. Bofill and P. Pulay, *J. Chem. Phys.*, 1989, **90**, 3637.
86 R. G. A. Bone and P. Pulay, *Int. J. Quantum Chem.*, 1992, **45**, 133.
87 P. Pulay and T. P. Hamilton, *J. Chem. Phys.*, 1988, **88**, 4946.
88 R. Fournier, *J. Chem. Phys.*, 1993, **99**, 1801.
89 P. C. Engelking and W. C. Lineberger, *J. Am. Chem. Soc.*, 1979, **101**, 5569.
90 ACESII (a program product of the Quantum Theory Project, University of Florida): J. F. Stanton, J. Gauss, J. D. Watts, M. Nooijen, N. Oliphant, S. A. Perera, P. G. Szalay, W. J. Lauderdale, S. R. Gwaltney, S. Beck, A. Balkova, D. E. Bernholdt, K-K. Baeck, P. Rozyczko, H. Sekino, C. Huber and R. J. Bartlett; integral packages: VMOL (J. Almlöf and P. R. Taylor), VPROPS (P. R. Taylor), ABACUS (T. Helgaker, H. J. A. Jensen, P. Jorgensen, J. Olsen and P. R. Taylor).
91 D. Danovich and S. Shaik, *J. Am. Chem. Soc.*, 1997, **119**, 1773.
92 A. P. Scott and L. Radom, *J. Phys. Chem.*, 1996, **100**, 16502.
93 D. Federov, T. Furlani, S. Koseki, M. W. Schmidt and M. S. Gordon, in preparation.
94 D. Danovich and S. Shaik, *J. Am. Chem. Soc.*, 1997, **119**, 1773.
95 J. Olsen, O. Christiansen, H. Koch and P. Jørgenssen, *J. Chem. Phys.*, 1996, **105**, 5082.
96 B. O. Roos and K. Andersson, *Chem. Phys. Lett.*, 1995, **245**, 215.
97 B. O. Roos, K. Andersson, M. P. Fülscher, L. Serrano-Andrés, K. Pierloot, M. Merchán and V. Molina, *THEOCHEM*, 1996, **388**, 257.
98 R. J. Bartlett, *Annu. Rev. Phys. Chem.*, 1981, **32**, 359.
99 C. W. Murray and E. R. Davidson, *Int. J. Quantum Chem.*, 1992, **43**, 755.
100 H.-J. Werner and P. J. Knowles, *J. Chem. Phys.*, 1988, **89**, 5803.
101 P. J. Knowles and H.-J. Werner, *Chem. Phys. Lett.*, 1998, **145**, 514.
102 IFORB = 2 in the GAMESS $MCQDPT input group.
103 S. Wilson, K. Jankowski and J. Paldus, *Int. J. Quantum Chem.*, 1985, **28**, 525.
104 ISELCT = 1 and THRWGT = 1.0d-6 in $MCQDPT in GAMESS.
105 B. Simon, *Int. J. Quantum Chem.*, 1982, **21**, 3.
106 G. B. Arfken and H. J. Weber, *Mathematical Methods for Physics*, Academic Press, New York, 4th edn., Section 6.5 in particular.
107 H-J. Werner and P. J. Knowles, *J. Chem. Phys.*, 1985, **82**, 5053.
108 P. J. Knowles and H-J. Werner, *Chem. Phys. Lett.*, 1985, **115**, 259.
109 Whether the units of radian^2 should be included in the denominator is debatable. For a description of angular units see the informative article: K. R. Brownstein, *Am. J. Phys.*, 1997, **65**, 605.

Paper 8/08518H